Numerical Investigations on Wind Flow over Complex Terrain

by

S. Ramechecandane and Arne Reidar Gravdahl

Reprinted from
WIND ENGINEERING
Volume 36, No. 3, 2012

Multi-Science Publishing Company
5 Wates way · Brentwood · Essex CM15 9TB · UK
Tel: +44(0)1277 224632 · Fax: +44(0)1277 223453
E-mail: mscience@globalnet.co.uk · Web Site: www.multi-science.co.uk

Numerical Investigations on Wind Flow over Complex Terrain

S. Ramechecandane[1] and Arne Reidar Gravdahl[2]
[1]Senior Engineer, Hydro Aluminium AS, Porsgrunn, Norway
[2]CEO WindSim AS, Tonsberg, Norway

Submitted March 14, 2012; Revised May 8, 2012; Accepted May 10, 2012

ABSTRACT

A comparison of three two-equation turbulence models namely the standard k-ε model, Renormalized Group Theory (RNG) k-ε model and the k-ω model of Wilcox for flow over three different types of topographies have been presented in this paper. The present work is also an attempt to propose best practices for simulating atmospheric boundary layer (ABL) flows over complex terrain. Numerical investigations are performed for three different topographies: (i) cosine Hill (ii) Bolund Hill and (iii) Askervein Hill. The commercial CFD solver PHOENICS and the wind farm design tool WindSim V-5.1.0 are used for solving the Reynolds Averaged Navier Stokes (RANS) equations with the turbulence closure. The profiles of velocity and turbulent kinetic energy obtained using the various turbulence models are compared with available experimental data. The numerical results clearly show the superiority of the k-ω model of Wilcox over the standard k-ε model and the RNG k-ε model for ABL flows. Though the velocity profiles obtained using all three models are alike there exists a significant variation in the turbulent kinetic energy profiles for the cases considered in this investigation. The models perform very well when the terrain orography is quite complex, except for the predictions on the leeward side of the Hill where the elliptic effects are more pronounced.

Keywords: Computational Fluid Dynamics, turbulence models, atmospheric boundary layer flows, wall functions, roughness length

NOMENCLATURE

c	ratio of the first and last element
G	Generation terms, [N/m^3]
h	boundary layer height, [m]
h^*	height of the element in the BFC grid, [m]
i	coordinate index
j	coordinate index
$k_{s,ABL}$	sand grain roughness for the ABL, [m]
k	turbulent kinetic energy, [m^2/s^2]
t	time, [s]
T	temperature, [K]
u^*	frictional velocity, [m/s]

[1]Corresponding author Email: Rameche.Candane.Somassoundirame@hydro.com Telephone: +47 9544 6874

U axial velocity, [m/s]
u_j velocity, [m/s]
x_i, x_j position, [m]
y_0 aerodynamic roughness length, [m]
y_P distance from the wall to the center point of the first cell, [m]
z_{agl} height above the ground level
z_0 roughness height, [m]

Greek symbols
$C\mu$ constant in the k-ε model
δ_{ij} Kronecker delta
ε turbulent dissipation rate, [m^2/s^3]
κ Von-Karman constant
μ dynamic viscosity of gas, [kg/m/s]
G_t turbulent dynamic viscosity, [kg/m/s]
ν kinematic viscosity of gas, [m^2/s]
ρ density, [kg/m^3]
ω specific dissipation rate, [1/s]

1. INTRODUCTION

Over the past few decades, Computational Fluid Dynamics (CFD) has emerged as a reliable tool for simulating a number of engineering problems. The application of CFD to wind related problems has attracted attention in the recent past. Wind induced loads on buildings, dams, historical monuments, stadiums and other structures depend on the velocity profile and the turbulence characteristics of the wind flow [1]. Wind induced dispersion of pollutants in urban locations, pedestrian level winds, urban heat island, and many more phenomena also depends mainly on the flow and turbulent characteristics of wind; The modeling of wind farms in complex terrain also requires a reliable prediction of wind conditions. The upstream condition such as the terrain orography and roughness length plays a key role in determining the velocity and kinetic energy profiles that the structures of interest encounter. The presence of a Hill or a building upstream may result in the formation of a Von-Karman vortex street which may have a positive influence on building ventilation by maximizing the air flow and reducing the energy consumption by electrical appliances [2]. The flow behavior such as flow attachment cum detachment, recirculation zones, vortex formation and shedding can have a significant impact of the power production of wind farms. The turbulent intensity is a parameter of high importance in high rise structures and also in the construction of the wind farms. Accurate CFD simulations of atmospheric ABL flows are essential for a wide variety of atmospheric studies. The accuracy of such simulations relies mainly on the grid generated, the boundary and initial conditions applied, the turbulence model chosen and the wall functions used [3]. These problems are explained in detail in the ensuing sections.

1.1. Grid generation

The most prevalent view in the CFD community is that the grid generation phase is the most difficult and time consuming part of a project. There are so many ways of grid generation and each has its own merits and demerits. Most of the commercial and open source grid generators available today are based on four main methods of grid generation (i) body fitted coordinate grid (ii) multi-block structured grid (iii) Cartesian grid on a global coordinate system and (iv) unstructured grid. The present work uses a body fitted coordinate grid owing

to its simplicity in implementation and ease of use. The main limitation with a body fitted coordinate grid for complex terrain is its inability to handle terrain inclination angles beyond 60–70°. The grid distribution along the vertical direction may follow an arithmetic or geometric progression. In the present study the grid is generated using an arithmetic progression. The grading follows an arithmetic sequence [4]:

$$h_i^* = h_{i-1}^* + \Delta h^* \tag{1}$$

Given n elements, the grading over an interval of length L is determined by the ratio of the first and last element size $\frac{h_i^*}{h_n^*} = c$. The additive constant Δh^* is the difference in size between two consecutive elements and the size of the first element is given by

$$\Delta h^* = \frac{L}{\frac{nc(n-1)}{1-c} + \sum_{i=1}^{n-1} i} \tag{2}$$

$$h_1^* = \frac{\Delta h^* c(n-1)}{1-c}. \tag{3}$$

The arithmetic sequence represents a convenient method for smooth grid construction with a desired grading. The commercial solver used for the present study uses a body fitted coordinate grid with an arithmetic sequence for grading along the vertical direction. The multi-block structured grid and the unstructured grid requires a bit of effort from the user side. The unstructured grid can be generated using a number of ways ranging from the quadtree/octree algorithm to the Delaunay triangulation and Voronoi's theorem. The area of grid generation itself has emerged into an area of research by itself. The suitability of a particular grid generation technique for the problem under investigation requires an in-depth analysis.

1.2. Initial and boundary conditions

The total time to convergence of a numerical solution is purely dependent on the initial guess. The usual practice is to patch the whole computational domain to values those are closer to the expected solution. In atmospheric flows the computational domains considered are too large in size and hence the computational time associated with such problems is high. In order to accelerate the convergence, it is a common practice to start with an initial profile for velocity and other turbulence quantities such as the turbulent kinetic energy and the turbulent dissipation rate/specific dissipation rate. In the present study, the log law profile is assigned to the velocity magnitude and polynomial curve fits are used for the turbulent kinetic energy and dissipation rate. If the inlet conditions are known from experiments then a Dirichlet condition can be applied at the inlet boundary. The outflow condition with a specified pressure is applied to the outlet boundaries. The profiles of velocity and turbulent quantities are assumed to be fully developed. The no slip wall boundary condition along with a wall function to account for the roughness length is set for the wall. The turbulence kinetic energy is set as zero at the ground. The top boundary condition can either be a no friction wall or a pressure boundary condition with fixed velocities in the case of atmospheric boundary layer flows. Based on the direction of flow the computational domain may have more than one inlet and outlet boundaries. It is also possible to extract the boundary conditions from a meso-micro scale coupling procedure. The boundary conditions are extracted from the meso-scale CFD

model or a Weather Research and Forecasting (WRF) model. These profiles may serve as true representatives of the actual conditions than the idealized profiles which are current industry practice.

1.3. Turbulence model

The availability of literature on turbulence models for simulating fluid flow problem is quite vast. The models can be broadly categorized as isotropic and anisotropic models. The isotropic models assume that the fluctuating velocity components in all the three directions are equal. Of the various turbulence models available for turbulence closure, the isotropic two equation models are quite lucrative from a computational point of view. The models are reasonably accurate and computationally less expensive. WindSim solves the equations for turbulent kinetic energy (k) and turbulent dissipation rate (ε)/turbulent frequency (ω) to represent flow dynamics over complex terrains. The simplest models of turbulence namely the two equation models are tested in the present study.

1.4. Wall function problems

In ABL flows, the wall functions are used as an effective substitute for actual roughness obstacles and are supposed to provide the same effect on the flow as these obstacles. The roughness in ABL flows can be expressed in two ways [1]:

1. Aerodynamic roughness length (y_0)
2. Sand grain roughness ($K_{s,\,\mathrm{ABL}}$)

A detailed literature review reveals that there exists a linear relationship between these two roughness quantities.

$$K_{s,ABL} = 30\,y_0 \tag{4}$$

Using eqn. (4) it can be seen that the sand grain roughness corresponding to high aerodynamic roughness assumes values those are extremely high and at times physically unrealistic. An aerodynamic roughness length of 1 m might yield an equivalent sand grain roughness of 30 m. In wind energy related studies, it is also not uncommon to work with aerodynamic roughness lengths of a couple of meters. Such values of aerodynamic roughness length might apparently lead to sand grain roughness of say 60 or 90 m.

In order to perform a proper CFD simulation of ABL flows the following requirements must be met (these conditions are reproduced from the works of Blocken et al. [1] for the sake of continuity):

1. A sufficiently high mesh resolution in the vertical direction close to the wall to ensure a reasonable value of wall $y^+\left(\frac{yu^*}{\nu}\right)$. Though the y^+ requirement (y^+ must range between 30 and 60) can be met in smaller computational domains with smooth walls, the presence of extremely rough walls might drastically influence the value of y^+ at the first cell from the wall. For an ABL flow the y^+ can be very large.
2. A horizontally homogeneous ABL flow in the upstream and downstream region of the domain. i.e., there should not be any formation of internal boundary layer (IBL).
3. A distance y_P from wall to the center point P of the first cell from the wall (bottom of domain) must be larger than the physical roughness height (sand grain roughness height k_s of the terrain ($y_P > k_s$); and
4. Knowing the relationship between the equivalent sand grain roughness height k_s and the corresponding aerodynamic roughness length y_0.

The first requirement is considered as important for all computational studies of flow near the surface of the earth (for instance, for pedestrian wind comfort studies). This requirement may be compromised to some extent in the case of wind resource assessment studies as the hub of the wind turbine lies at an altitude of say 60 m i.e., quite far from the ground. The second requirement implies the insertion of wall functions to account for ground roughness into the simulation to prevent streamwise gradients in the flow. The third requirement implies that it is not physically meaningful to have grid cells with center points within the physical roughness height. This is a very important condition to be satisfied but quite often ignored, in cases where the physical roughness/sand grain roughness goes to values as high as 30 or 60 m one cannot fix the first cell at a height of 60 or 120 m.

Say, the aerodynamic roughness for a terrain with grass is 0.03 m $y_0 = 0.03$ m then the sand grain roughness $k_s = 30\ y_0 \Rightarrow k_s = 0.9$ m

The center point of the first cell y_P must be greater than the physical roughness height k_s.

Hence, y_P~1 m this leads to a first cell thickness of 2 m and hence the possibility of having 3 to 4 control volumes within the first 1 m height from the wall is unimaginable for ABL flows, especially when working with sand grain roughness. A possible means of getting rid of this problem would be to work with the wall functions those are formulated for the aerodynamic roughness length itself (y_0 wall functions).

2. MATHEMATICAL FORMULATION

Using Reynolds averaging, the continuity and momentum equations turn out to be

$$\frac{\partial \rho}{\partial t} + \frac{\partial}{\partial x_i}(\rho u_i) = 0 \tag{5}$$

$$\frac{\partial}{\partial t}(\rho u_i) + \frac{\partial}{\partial x_j}(\rho u_i u_j) = -\frac{\partial p}{\partial x_i} + \frac{\partial}{\partial x_j}\left[\mu\left(\frac{\partial u_i}{\partial x_j} + \frac{\partial u_j}{\partial x_i} - \frac{2}{3}\delta_{ij}\frac{\partial u_i}{\partial x_j}\right)\right] + \frac{\partial}{\partial x_j}\left(-\rho u_i^* u_j^*\right). \tag{6}$$

The Reynolds stresses $\rho u_i' u_j'$ in the eqn. 6 must be modeled in order to close the equation. A common method employs the Boussinesq hypothesis to relate the Reynolds stresses to the mean velocity gradients

$$-\rho u_i' u_j' = \mu_t\left(\frac{\partial u_i}{\partial x_j} + \frac{\partial u_j}{\partial x_i}\right) - \frac{2}{3}\delta_{ij}\left(\mu_t \frac{\partial u_i}{\partial x_i} + \rho k\right). \tag{7}$$

The advantage of this approach is the relatively low computational cost associated with the computation of the turbulent viscosity (μ_t).

2.1. Standard *k-ε* model and RNG *k-ε* model

In the case of the standard k-ε model and RNG k-ε model, two additional transport equations (for the turbulent kinetic energy k, and the turbulent dissipation rate ε) are solved, and μ_t is computed as a function of k and ε.

$$\frac{\partial}{\partial t}(\rho k) + \frac{\partial}{\partial x_j}(\rho k u_i) = \frac{\partial}{\partial x_j}\left[\alpha_k\left(\mu_{eff}\frac{\partial k}{\partial x_j}\right)\right] + G_k - \rho\varepsilon \tag{8}$$

$$\frac{\partial}{\partial t}(\rho \varepsilon) + \frac{\partial}{\partial x_j}(\rho \varepsilon u_i) = \frac{\partial}{\partial x_j}\left[\alpha_\varepsilon\left(\mu_{eff}\frac{\partial \varepsilon}{\partial x_j}\right)\right] + C_{1\varepsilon}G_k\frac{\varepsilon}{k} - C_{z\varepsilon}\rho\frac{\varepsilon^2}{k} - R_\varepsilon \tag{9}$$

$$\mu_t = \rho C_\mu \frac{k^2}{\varepsilon} \tag{10}$$

The disadvantage of the Boussinesq hypothesis as presented is that it assumes μ_t is an isotropic scalar quantity, which is not strictly true. The major parameters that differentiate RNG k-ε model from the standard k-ε model are the constants involved in the equations (8) and (9) and the term R_ε that is present in the right hand side of eqn (9), and is given by.

$$R_\varepsilon = \frac{C_\mu \rho \eta^3 \left(1 - \frac{\eta}{\eta_0}\right)}{1 + \beta \eta^3} \frac{\varepsilon^2}{k}. \tag{11}$$

Where $\eta = \frac{Sk}{\varepsilon}$; $\eta_0 = 4.38$; $\beta = 0.012$

The values of constants involved in eqns (8), (9) and (10) are given in table. 1

The term G_k representing the production of turbulent kinetic energy is modeled as

$$G_k = -\overline{\rho u_i' u_j'} \left(\frac{\partial u_j}{\partial x_i}\right). \tag{12}$$

2.2. k-ω model of Wilcox

In the case of the k-ω model, two additional transport equations (for the turbulent kinetic energy k, and the turbulent frequency ω) are solved, and μ_t is computed as a function of k and ω. The turbulent frequency or the specific dissipation rate can be expressed as a ratio of ε to k.

$$\frac{\partial}{\partial t}(\rho k) + \frac{\partial}{\partial x_j}(\rho k u_i) = \frac{\partial}{\partial x_j}\left[\alpha_k \left(\mu_{eff} \frac{\partial k}{\partial x_j}\right)\right] + G_k - Y_k + S_k \tag{13}$$

$$\frac{\partial}{\partial t}(\rho \omega) + \frac{\partial}{\partial x_j}(\rho \omega u_i) = \frac{\partial}{\partial x_j}\left[\alpha_k \left(\mu_{eff} \frac{\partial \omega}{\partial x_j}\right)\right] + G_\omega - Y_\omega + S_\omega \tag{14}$$

and μ_t is given by

$$\mu_t = \rho \alpha^* \frac{k}{\omega}. \tag{15}$$

The coefficient α^* damps the turbulent viscosity causing a low Reynold's number correction. In the high Reynolds number form of the k-ω model $\alpha^* = 1$ and hence

$$\mu_t = \rho \frac{k}{\omega}. \tag{16}$$

The production terms of turbulent kinetic energy and turbulent frequency in k-ω model are similar to those present in the k-ε model. The k-ω model is reported to perform better in

Table 1: Constants involved in the RNG $k - \varepsilon$ model

C_μ	$C_{1\varepsilon}$	$C_{2\varepsilon}$	α_k	α_ε	η_0	β
0.0845	1.42	1.68	1.39	1.39	4.38	0.012

transitional flows and in flows with adverse pressure gradients. The k-ω model is numerically very stable and it tends to produce converged solutions more rapidly than the standard k-ε model or the RNG k-ε model. The main weakness of the k-ω model is that unlike the variants of the k-ε model, it is sensitive to the free stream boundary condition for ω in free shear flows. The cells are contiguous, i.e., they do not overlap one another and completely fill the domain. Dependent variables and other properties are principally stored at the cell centroid although they may be stored on faces or vertices. The spatial discretization is carried out using a hybrid discretization scheme (a combination of central differencing and upwind differencing schemes based on the cell Peclet number) and the temporal discretization is by using an Euler implicit scheme. In addition to the discretization schemes, particular emphasis has also been placed on the grid's refinement because, besides reducing the spatial discretization error, fine grids improve the topography's resolution, adding surface detail that would be otherwise lost.

The wind fields are determined by solving the Reynolds Averaged Navier-Stokes equations (RANS). The two equation turbulence models are used to achieve turbulence closure. Since the equations are non-linear the solution procedure is iterative. Starting with the initial conditions, which are guessed estimations, the solution is progressively resolved by iteration until a converged solution is achieved. The flow variables those are solved are the pressure (p), velocity components (u, v and w), turbulent kinetic energy (k) and the turbulent dissipation rate (ε) or turbulent specific dissipation rate (ω). The initial conditions considered for the present investigation are taken from the experimental data provided by DTU [2]. The atmosphere is assumed to be a neutral atmosphere and thereby the effect of thermal stratification is not taken into account. In the case of a neutral atmosphere the wind profiles are logarithmic. The well-known logarithmic profile at the computational boundary is given by

$$U = \frac{u^*}{K}\log\left(\frac{z_{agl}}{z_0}\right) \tag{17}$$

Where, $K = 0.41$ is the Von-Karman constant; u^* is the frictional velocity; z_{agl} is the height above the ground level given by $z_{agl} = z - gl$ ($gl = 0.75$ m) and z_0 is the roughness height. The turbulent kinetic energy is set to be constant with height from the experimental data

$$\frac{k}{u^{*2}} = 5.8 \tag{18}$$

$$\varepsilon = \frac{u^{*3}}{\kappa(z + z_0)} \tag{19}$$

$$\omega = \frac{\varepsilon}{C_\mu k}. \tag{20}$$

The simulations are run with dry air and the properties of air are set to be: density (ρ) = 1.229 kg/m^3, dynamic viscosity (μ) = 1.75×10^{-5} Kg/m/s at a corresponding temperature of 15°C.

3. RESULTS AND DISCUSSION

3.1. Single cosine hill

Variation of wind speeds over a single cosine Hill serves as a validation case for the k-ω turbulence model used in the present study. A comparison of the various two equation models made the authors to be more inclined towards the k-omega model and also to advocate this two equation model to be the most suitable alternative to simulate flows with strong

separation and recirculation. Speed up ratios obtained for the single cosine Hills (2 cases are considered) from the present study are compared with the boundary layer wind tunnel (BLWT) and two dimensional results of Carpenter and Locke [5]. As the intention of the present analysis is to simulate flow over large computational domains, the topographies considered for the present investigation range from a few metres to the order of kilometres.

The three dimensional body fitted coordinate grid created for the cosine Hill considered for the present investigation is shown in Fig. 1. The size of the computational domain considered is 4000 m long, 2600 m broad and 400 m high. Two sizes of cosine Hills are considered for the present study (a) a cosine Hill of 200 m height and 400 width/length – a shallow Hill; (b) a cosine Hill of 200 m height and 200 width/length – a steep Hill. The grid spacing along the x and y direction is set to approximately 10 m. A grid dependent study has been carried out using a number of simulations to arrive at the optimal grid size. The grid distribution along the vertical direction is non-uniform and follows an arithmetic progression. The ratio between the last and the first cell from the wall is 0.1. The roughness height on the cosine Hill is taken as 0.03 m (this roughness value corresponds to pastures/natural grassland). The inclination angle and the second order derivative for the cosine Hill (a cosine Hill of 200 m height and 400 width/length) are presented in Figs. 2(a) and 2(b). The velocity contours obtained from the present simulation for the cosine Hill is presented in Fig. 3.

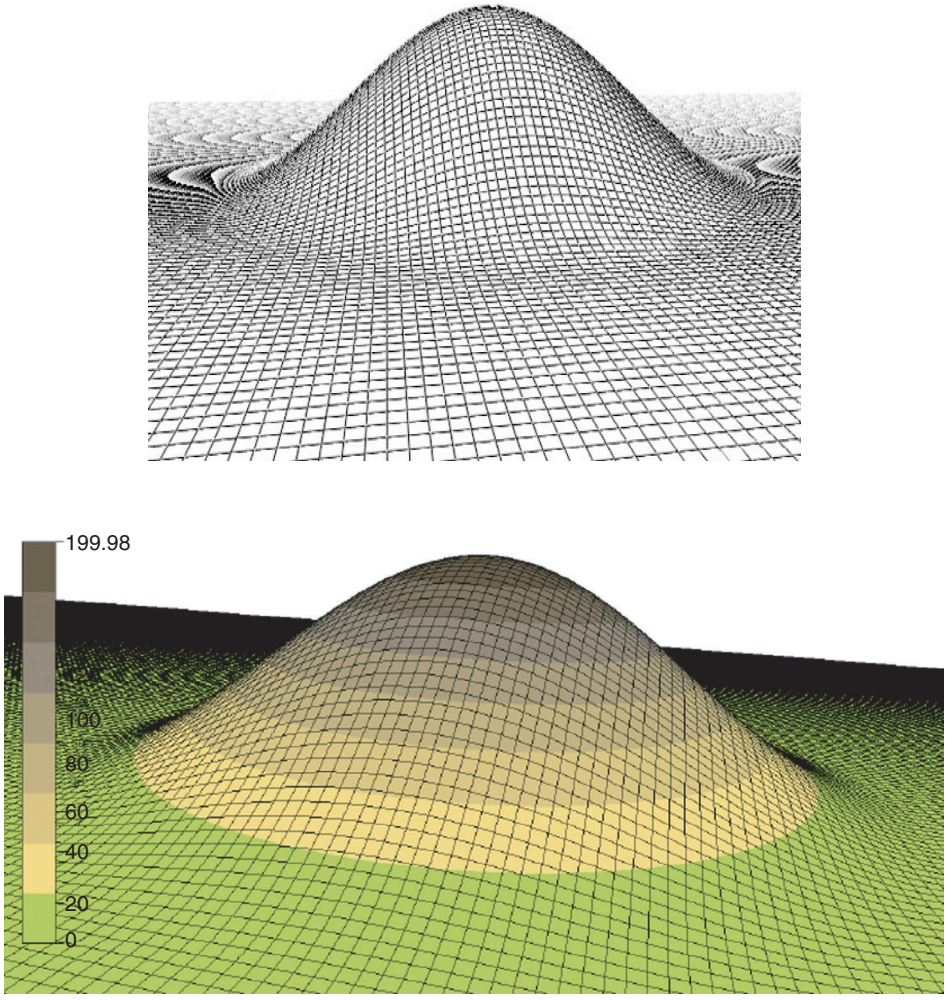

Figure 1: (a) BFC Grid Generated for the Cosine Hill (b) Contours of altitude.

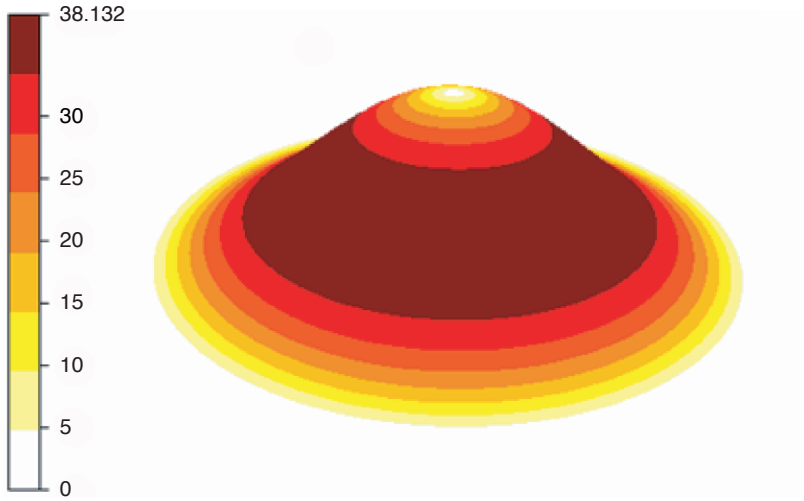

(a) Inclination angle, deg

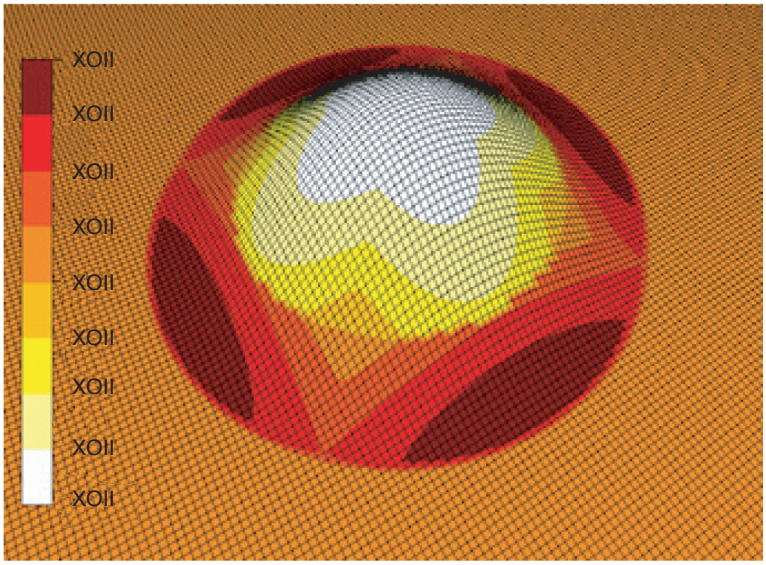

(b) Second order derivative

Figure 2: (a) Inclination angle in degrees and (b) Second order derivative for the cosine Hill.

The flow patterns on the leeward side of the Hill show the formation of two vortices on both the sides of the Hills, this feature is not observed when the grid points are coarse. These vortices can be the starting point of a Von Karman vortex street and it can be clearly seen from the contour plot that the velocity magnitude in these regions are quite high as compared to the wake region on the leeward side of the cosine Hill. The formation of the Von Karman street can be more clearly seen when transient simulations are performed for these cosine Hills. The formation of a Von Karman street when wind flows over complex terrain or structures such as buildings can have a positive or a negative impact on the structures present at the regions of vortex formation. The Von Karman vortex street can result in natural ventilation of buildings which can save energy due to reduced running of electrical appliances [2]. A comparison of the speed up ratios at the cosine Hill crest obtained from the present investigation with those of Carpenter and Locke [5] is presented in Fig. 4(a) and 4(b). The

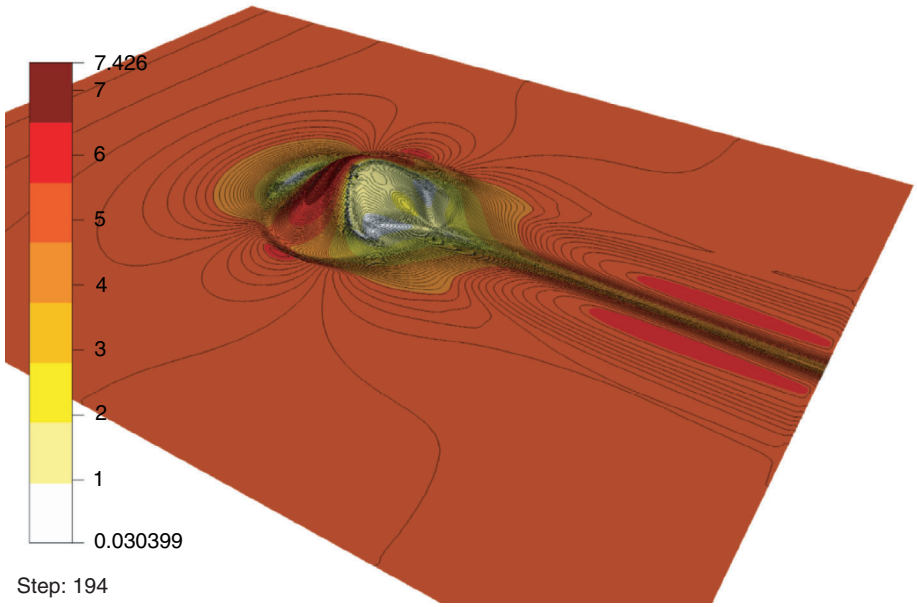

Figure 3: Contours of velocity magnitude at the first cell from the wall.

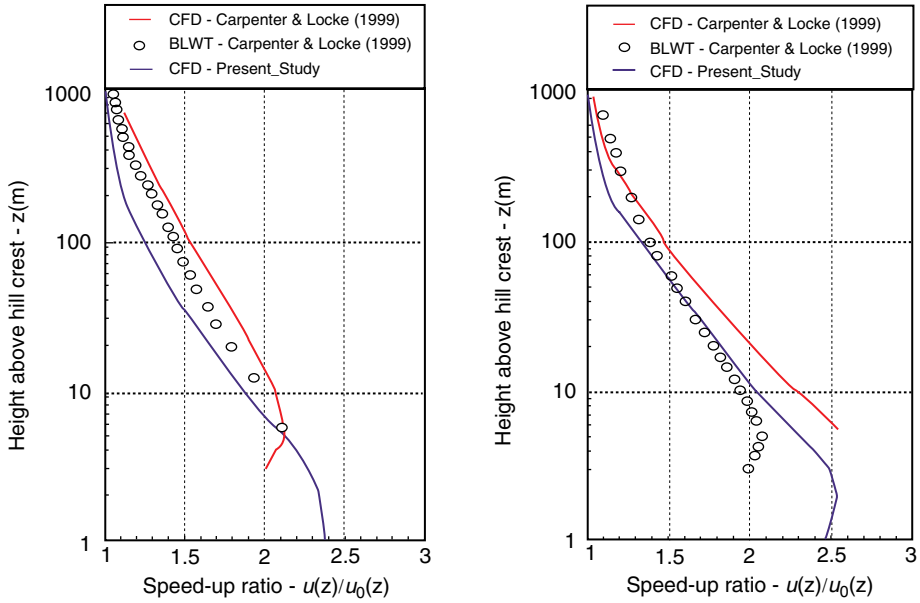

Figure 4: Comparison between BLWT (Carpenter and Locke (1999), 2 Dimensional CFD (Carpenter and Locke (1999) and the present 3 dimensional analysis speed up ratios at crest of (a) Cosine Hill (200 m high × 200 m Long) (b) Cosine Hill (200 m high × 400 m Long).

results obtained using the present study are in good agreement with the BLWT data of Carpenter and Locke [5]. The total number of grids used for the present investigation is 3 million and hence provides numerical results those are more reliable than the two dimensional results presented in previous studies [1, 5].

3.2. Bolund hill

The Bolund experiment performed during a 3 month period beginning in 2007 and ending in 2008 provides a dataset for validating models of flow over complex terrains. Bolund is a 12 m

high coastal Hill located in Denmark [6]. Figure 5 shows the contours of elevation for the Bolund Hill. A detailed description of the Bolund experiment can be seen from the technical report by Risø laboratory of the Denmark Technical University (DTU) [7].

Fig. 6 shows an overview of the Bolund orography and the location of the ten measurement masts used to support the measuring instruments. The Bolund Hill is covered by grass with an aerodynamic roughness length of 0.015 m and the surrounding water is assigned an aerodynamic roughness length of 0.0003 m. Though the water roughness will vary with wind speed and direction a roughness length of 0.0003 m is more realistic from a computational point of view. The measurement masts are numbered 0-9 and are shown in Fig. 6 with red dots. The geometrical shape of the Bolund Hill has a vertical escarpment and hence makes the Bolund case a challenging problem to the CFD solvers available in the

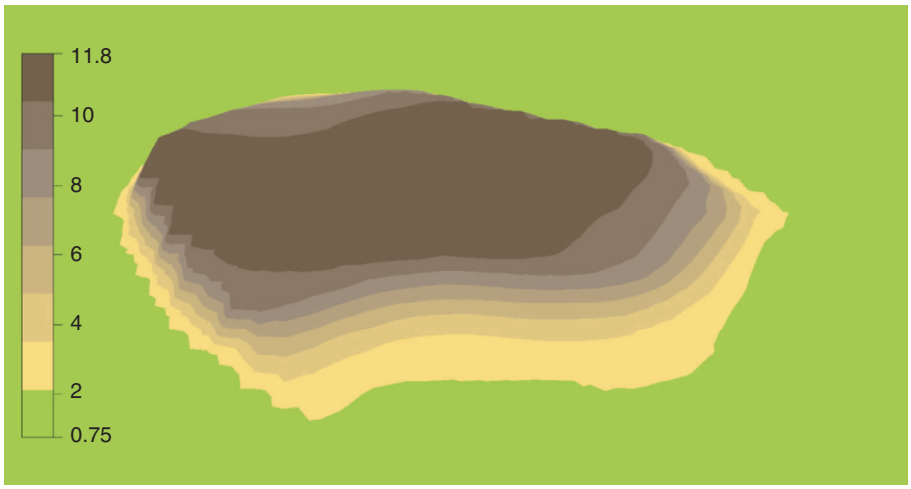

Figure 5: Contours of elevation for the Bolund Hill.

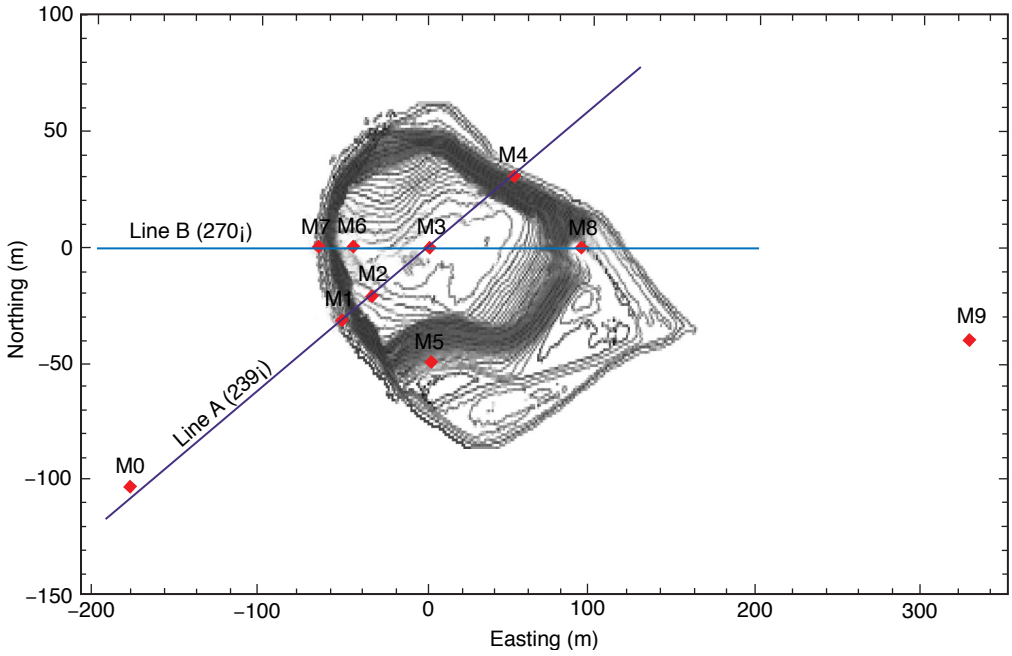

Figure 6: Bolund orography and the location of the met masts.

market. The validation of the turbulence model requires difficult test cases with steeper elevation than the widely experimented sinusoidal/cosine Hill (explained in section 3.1). The measurement data from the Askervein Hill serves as a validation case for most flow modeling problems over complex terrains to date. The measurement masts located in water (M0 and M9) provides the required information about the inlet boundary conditions to perform simulations. During the campaign, velocity and turbulence were collected simultaneously from 35 anemometers (23 sonics and 12 cups) on ten masts. The measurement masts were located along two lines 239° and 270° respectively. The measurement masts located in water were equipped with cup anemometers at altitudes of 2 m, 5 m, 9 m and 15 m to measure the mean velocity profile and sonic anemometers were placed at an altitude of 5 m on both the masts to measure the turbulence.

3.2.1. Grid Generation for the Bolund Hill

The grid generated for the Bolund Hill is shown in Fig. 7. The grid generated for the terrain is a body fitted coordinate grid. The grid is refined in the areas closer to the Hill to ensure that spacing along the x and y directions varies from 2.1 m in the refinement areas to 25.1 m in regions far from the Hill. The grid along the vertical direction is also non-uniform and follows an arithmetic progression. The first cell is located at a distance of 1 m to justify the usage of wall functions to account for the roughness length. The first cell from the wall is located at a distance that is high enough to justify the usage of wall functions to account for the terrain roughness. The open area between the ground and upper boundary of the computational domain is calculated as the model is traversed in west-east and south-north direction. If the ratio between the minimum and maximum open area becomes too small, blocking effects might lead to unphysical speed-ups. As a rule of thumb the fraction between the minimum and maximum open area between the ground and the upper boundary, calculated as the model is traversed in west-east and south-north direction, should be larger than 0.95, i.e. (Open area Minimum)/(Open area Maximum) >0.95.

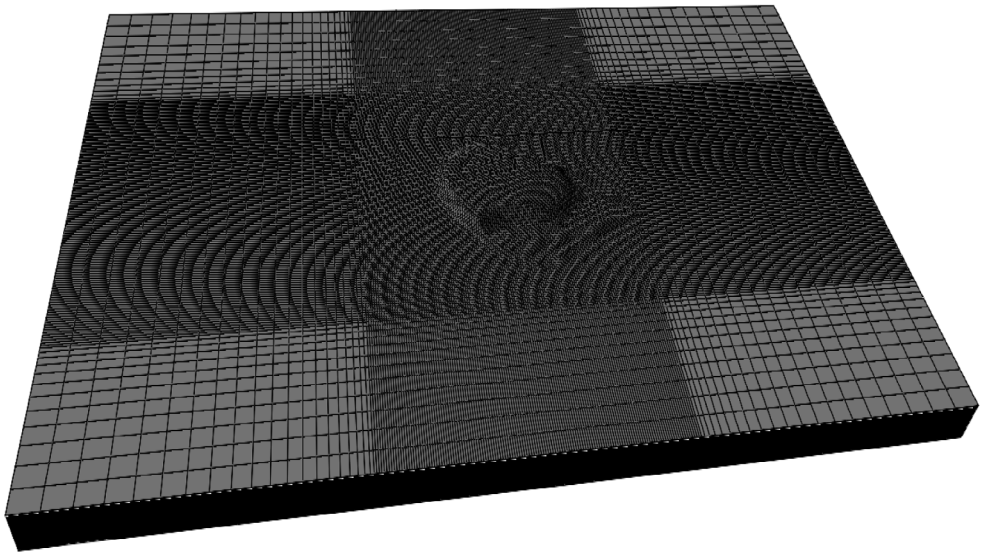

Figure 7: Body fitted coordinate (BFC) grid generated for the Bolund Hill.

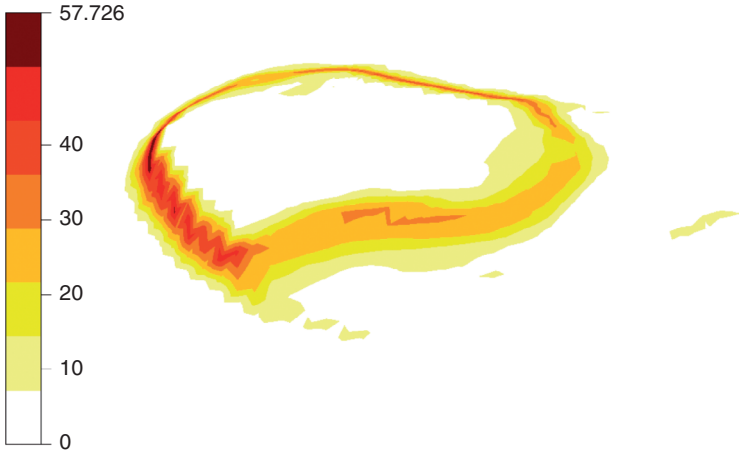

Figure 8: Contours of inclination angle for the Bolund Hill.

The total number of elements/cells used for the present study is approximately 1.5 million. The contours of inclination angle calculated using the grid generated is shown in Fig. 8. The angle of inclination may vary significantly with respect to the number of cells used. The angle of inclination parameter is of most interest in the case of BFC grids. As a rule of thumb the angle of inclination should not exceed 60°-70°. The higher the angle of inclination the more skewed the grid becomes and hence the error associated with these grids also shoots up. The maximum angle of inclination in the vertical escarpment of the Bolund Hill reaches a maximum value of 57.7° for the grid considered in the present investigation. It is also a common practice to keep the second order derivative of the terrain elevation within a certain value to ensure convergence.

When the flow direction is 270° the computational domain has a single inlet (the face/boundary facing the west) and four outlets (pressure specified). The ground is set as a wall with a wall function to account for the roughness length. If the flow is entering at 239° then the computational domain has two inlets (west and the south boundaries) and two outlets (north and east boundaries). The velocity at the inlet is set to be 14 m/s and the turbulence kinetic energy is calculated using eqn. (18) with a frictional velocity of 0.4 m/s (from experiment).

3.2.2. Numerical Analysis

Two cases have been considered for the present investigation wherein the flow enters from the westerly (270°) and south-westerly (239°) directions. Three of the widely used two-equation turbulence models (the standard k-ε model, Renormalized Group Theory (RNG) k-ε model and the k-ω model of Wilcox) have been considered for the present analysis. A comparison of the results obtained from these models with the experimental data is made. For, the sake of brevity, not all the contour plots obtained from the present study are shown in this section. Two representative plots that are truly representative of all the contour plots obtained using the present study, are shown in Fig. 9 and 10. Figures 9 and 10 present the contours of velocity magnitude and turbulent kinetic energy for an inflow angle of 239°. A comparison of the results obtained using the present simulations with the experimental data are presented in Figs. 11-14. Fig. 11(a)-11(e) present a comparison between the velocity magnitude obtained using the various turbulence models with experimental data. It is clearly evident from the plots that the velocity magnitude determined using the various turbulence

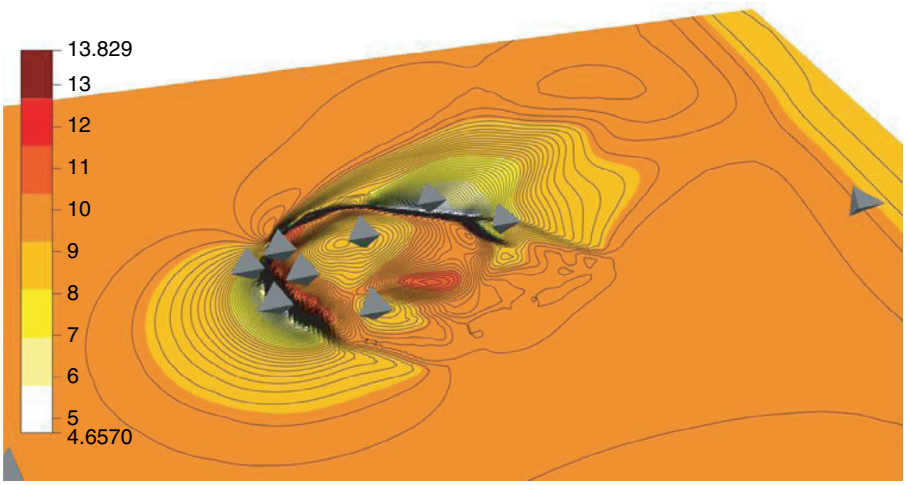

Figure 9: Contours of velocity magnitude ($m^2 s^{-1}$) at an altitude of 5 m above the Bolund Hill (flow enters at 239°).

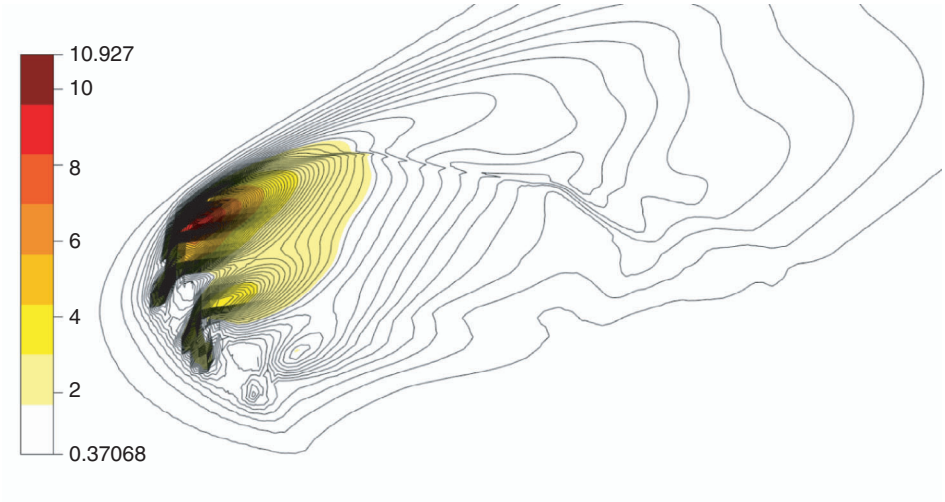

Figure 10: Contours of turbulent kinetic energy ($m^2 s^{-2}$) at an altitude of 5 m above the Bolund Hill (flow enters at 239°).

models are in close agreement with the experimental data. It is to be noted that the experimental data from Mast-4 that is located on the leeward side of the Hill (when the flow is aligned to 239°) shows the maximum discrepancy with the predicted values. This can be attributed to the strong recirculation zone that is formed on the leeward side of the Hill. From the velocity magnitude plots one would be forced to conclude that the results obtained using the two-equation models are reasonably accurate and the choice of the models does not influence the numerical results. A comparison of the turbulent kinetic energy obtained using the present simulations with experiments for a wind direction of 239° are presented in Figs. 12(a) - 12(e). From the plots of turbulent kinetic energy it can be seen that the predictions of the k-ω model of Wilcox are in close agreement with the experimental data. The mast-2 which is located on the crest of the Hill (where the speed up occurs) shows a tremendous increase in the turbulent kinetic energy as shown in Fig. 12(b). The results obtained using the

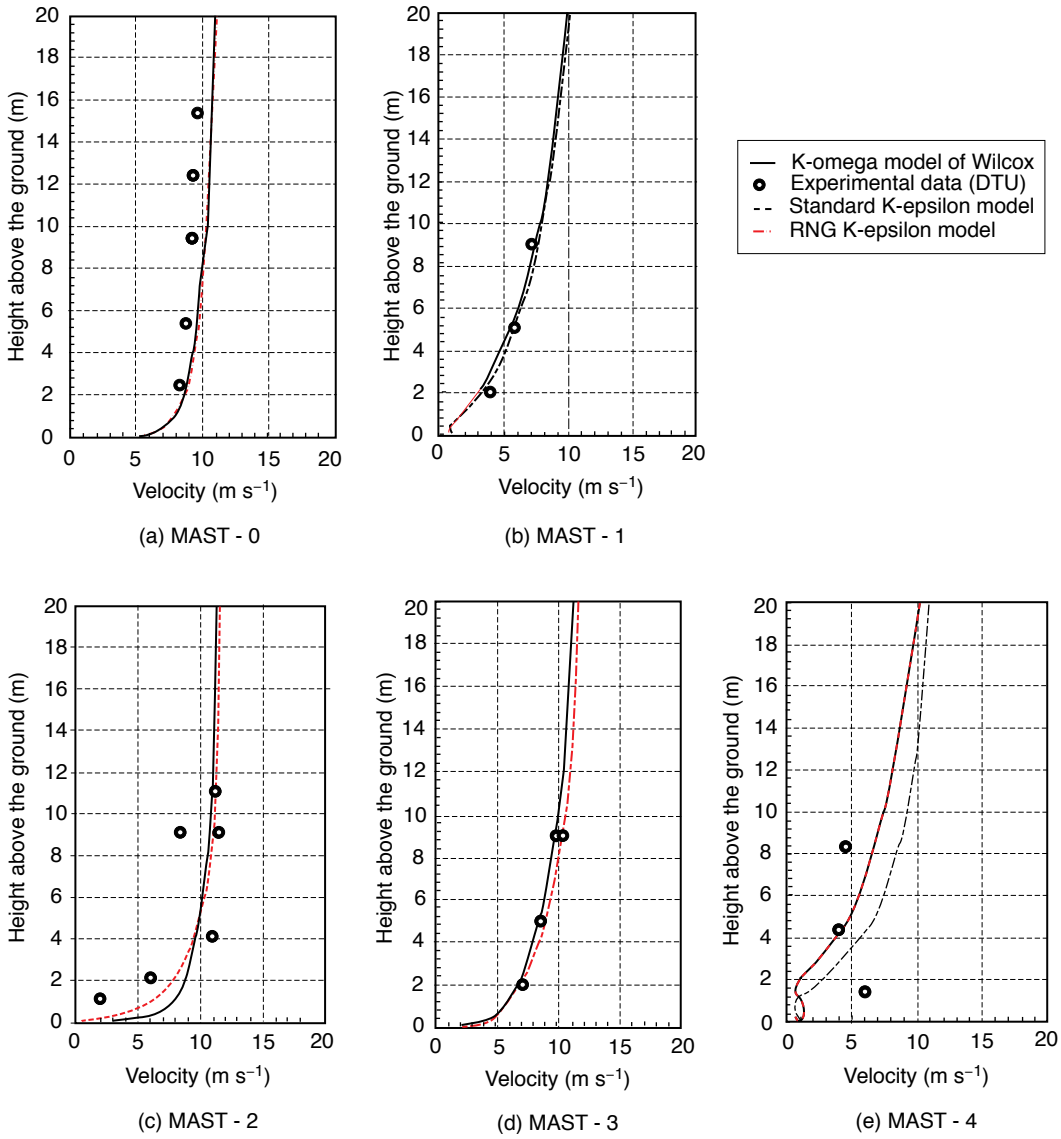

Figure 11: Comparison of velocity magnitude obtained using the present simulations with experiments for a wind direction of 239° (a) MAST-0; (b) MAST-1; (c) MAST-2; (d) MAST-3; (e) MAST-4.

k-ω model of Wilcox, are in close agreement with the experimental data in comparison to the standard and RNG k-ε models. When the flow takes place at 270° the velocity magnitude and the turbulent kinetic energy predicted using the turbulence models are in close agreement with the experimental data. Figures 13 and 14 present the results obtained using the various two equation models for a flow direction of 270°. In both the cases, it is seen that the results obtained for the leeward side of the Hill are nowhere close to the experimental data.

3.3. Askervein hill

The Askervein experiments carried out in the early 1980s [8, 9] still remain a reliable source of information for validating the flow models in ABL flows. Despite the many studies after this field measurement, to fully replicate the Askervein flow by CFD simulations is still a major challenge [10]. Though many studies on the Askervein Hill exist a comparison of the various

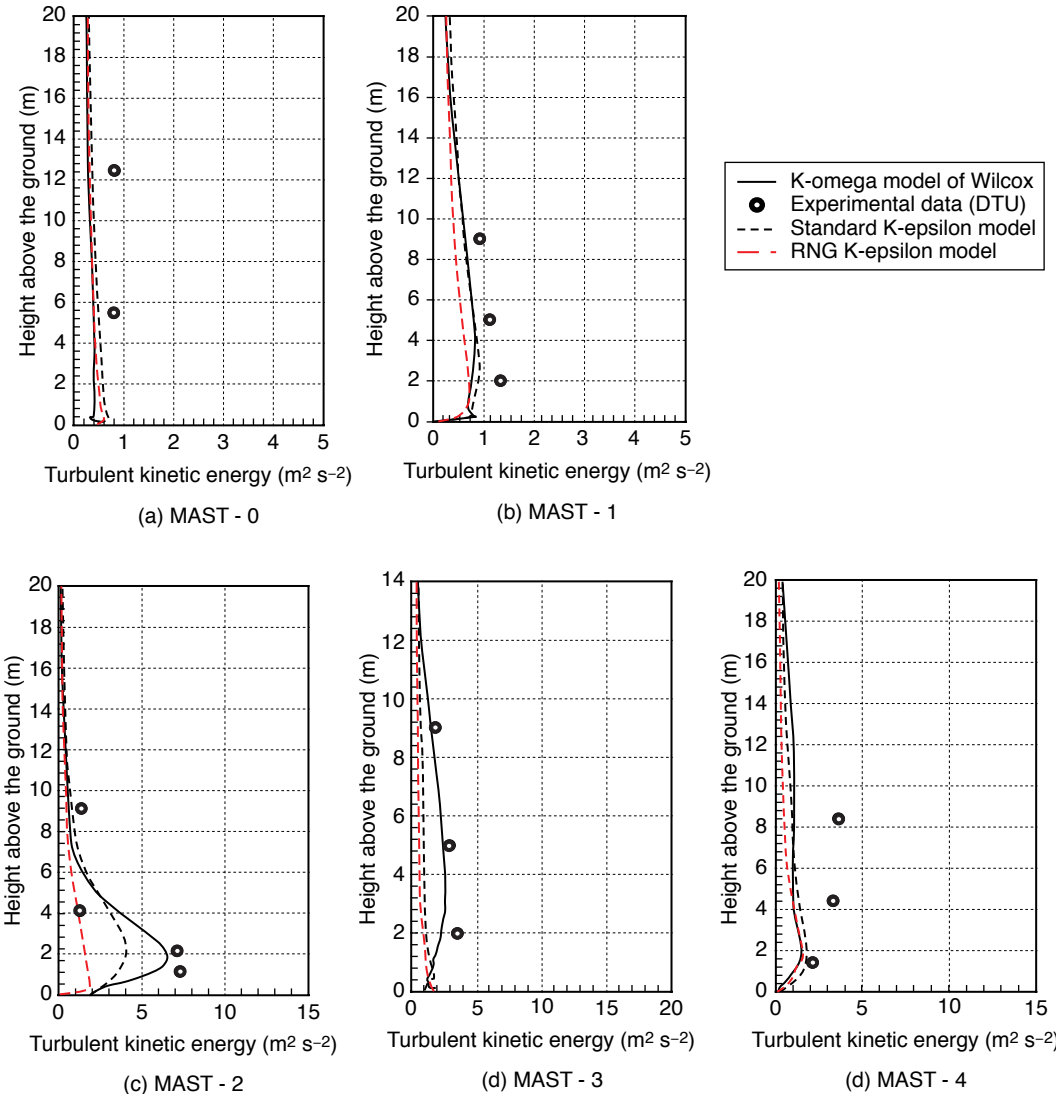

Figure 12: Comparison of turbulent kinetic energy obtained using the present simulations with experiments for a wind direction of 239°(a) MAST-0; (b) MAST-1; (c) MAST-2; (d) MAST-3; (e) MAST-4.

two-equation turbulence models has not been documented so far. Figure 15 shows the topography of the Askervein Hill with the three lines of measurement (ASW-ANE; AASW-AANE; BSE-BNW). The flow enters from an angle of 210° (from south-west directions) and leaves from the north-east directions. The domain considered for the present investigation is 3000 m (long) × 3000 m (wide) × 400 m (high) in size. The domain size is set in a way that the boundary conditions do not affect the flow behavior inside the regions of interest. The Askervein hill is nearly elliptic with a major and minor axes of roughly 1000 and 2000 m. The highest (ht) is 116 m above the surrounding terrain and the central point of the hill, along the major axis, is called point 'cp'. The points 'ht' and 'cp' are shown in Fig. 15.

3.3.1. Grid Generation for the Askervein Hill

The results presented by Castro et al [10] show that a coarse grid itself is sufficiently fine enough to calculate the speed up on the Hill top (10 m above ground). In the present study, a very fine grid is used for the complete investigation with a wall function which assumes a uniform roughness on the complete Hill. The grid generated for the present investigation along with the elevation map

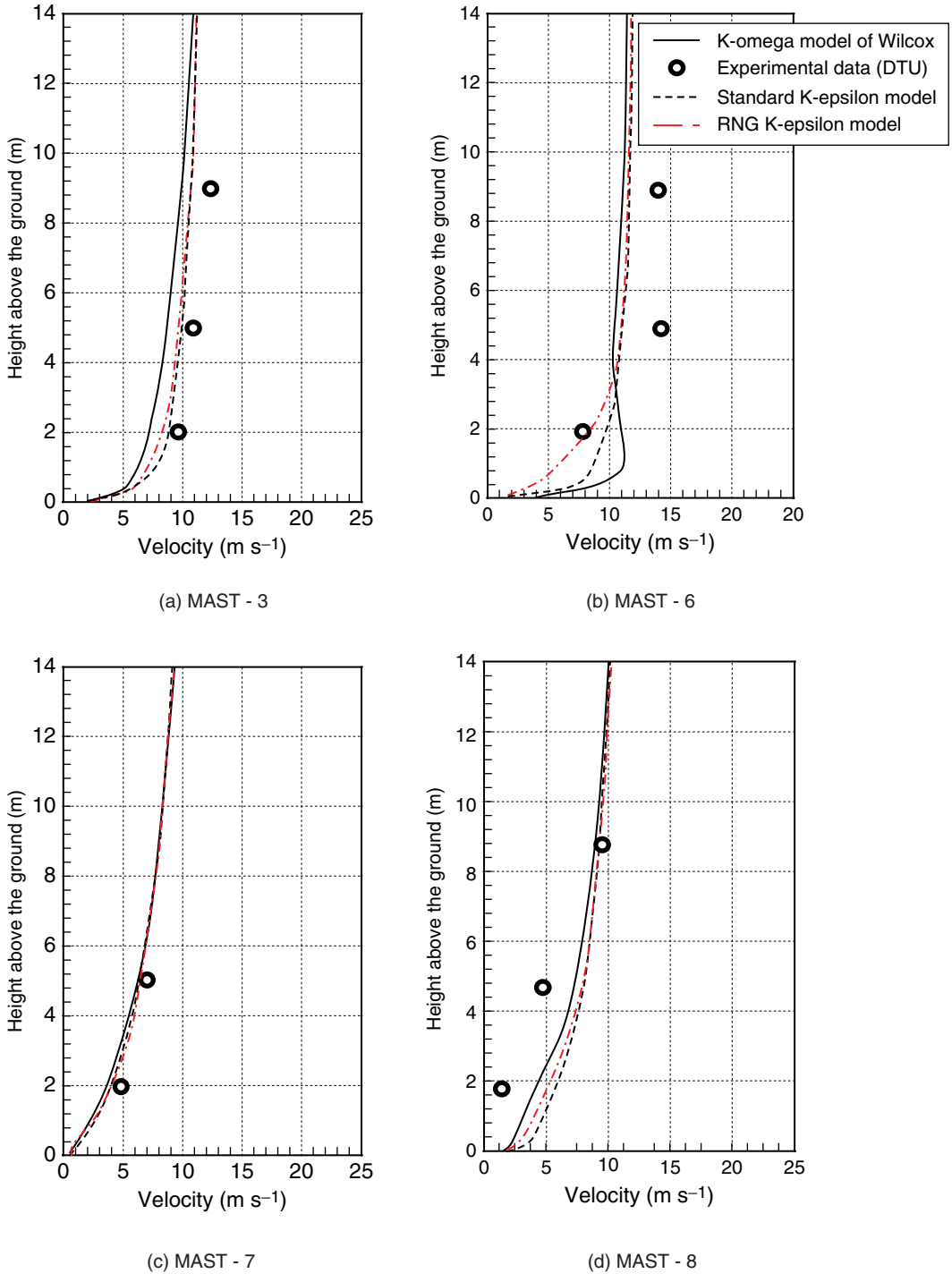

Figure 13: Comparison of velocity magnitude obtained using the present simulations with experiments for a wind direction of 270° (a) MAST-3; (b) MAST-6; (c) MAST-7 and (d) MAST-8.

is shown in Fig. 16. The BFC grid is refined close to the terrain to capture flow behavior in the vicinity of the Hill. The grid spacing along the x and y direction ranges from 25 m to 150 m. The aspect ratio along the vertical direction is kept as 0.1 to generate a grid that is sufficiently fine close to the ground. The first cell is located in a way that the usage of wall functions to account for wall roughness is justified. The wind direction for the present investigation is set to be 210° (similar to the investigation by Castro. et al [10]) and the boundary conditions cum initial conditions are similar to the ones assumed earlier in the case of the Bolund Hill.

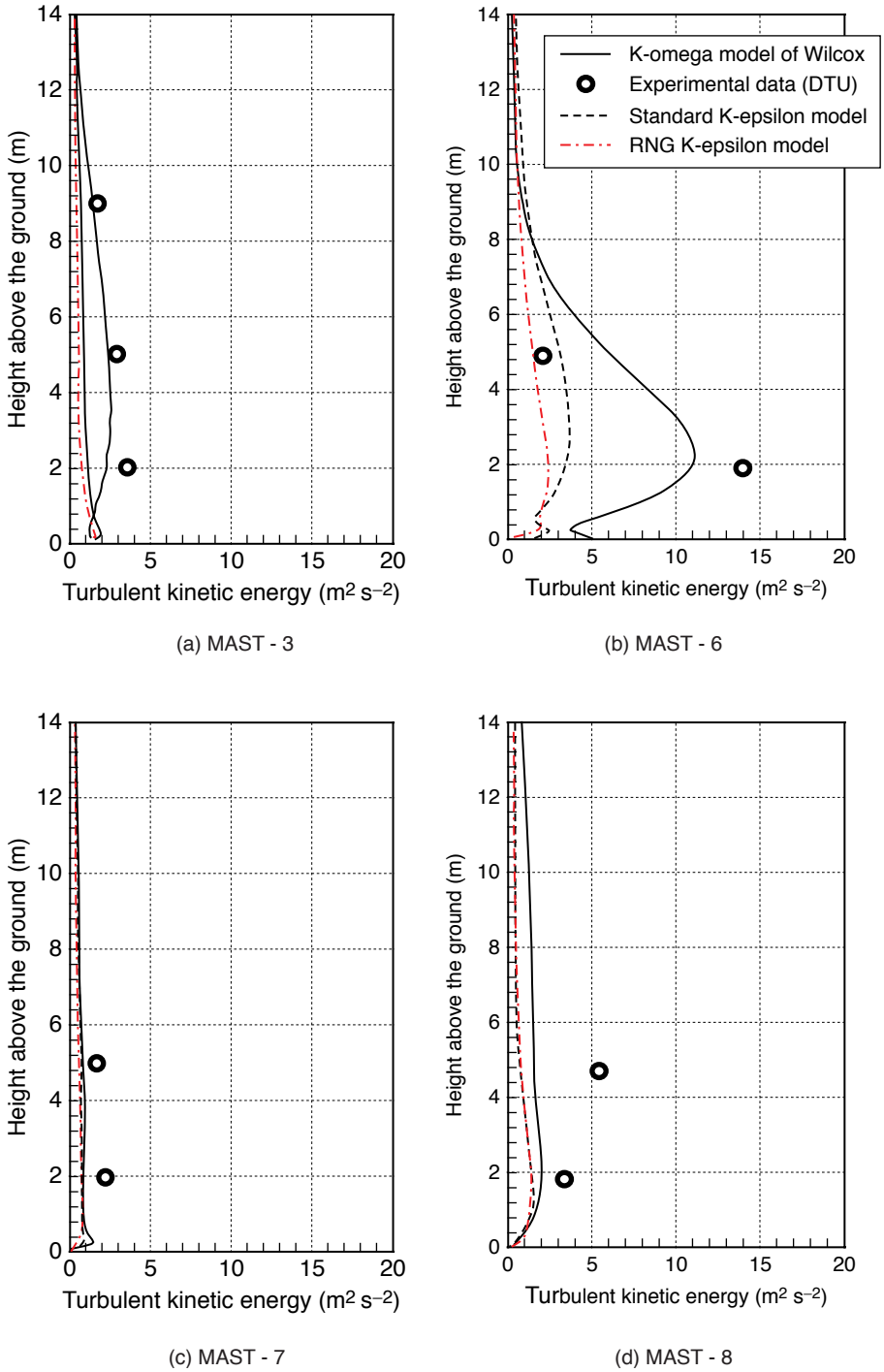

Figure 14: Comparison of turbulent kinetic energy obtained using the present simulations with experiments for a wind direction of 270°(a) MAST-3; (b) MAST-6; (c) MAST-7 and (d) MAST-8.

3.3.2. Boundary and Initial Conditions

The boundary close to the ground is modeled by a rough surface and a rough wall function is used to account for the terrain roughness. In the present work the velocity profiles are taken as idealized logarithmic profiles given by

$$U = \frac{u^*}{\kappa} \log\left(\frac{z_{agl}}{z_0}\right) \tag{21}$$

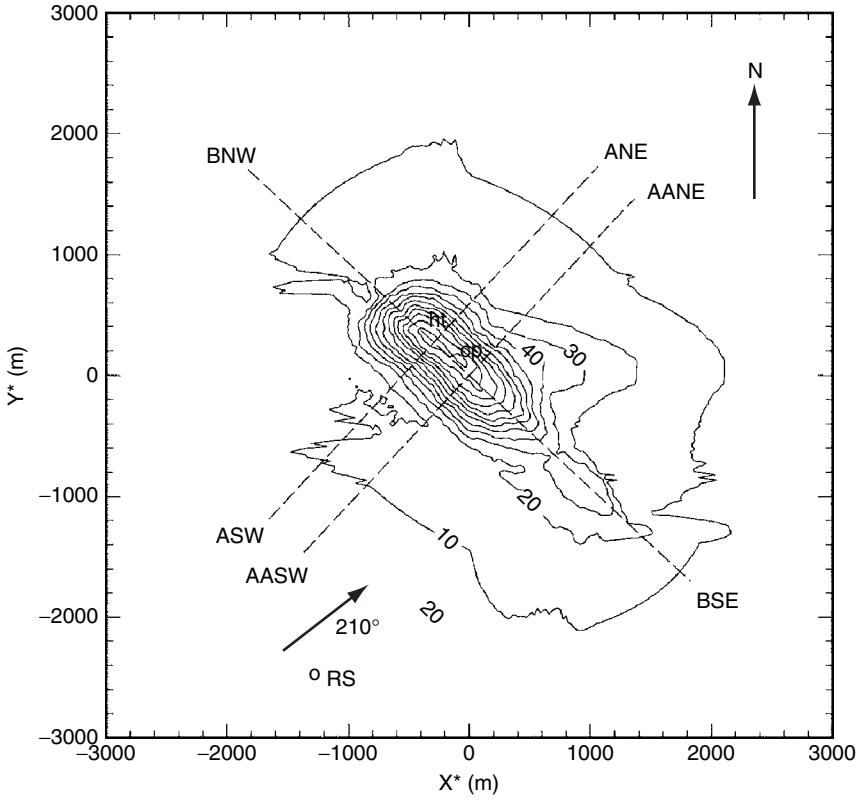

Figure 15: Askervein Hill Topographic Map.

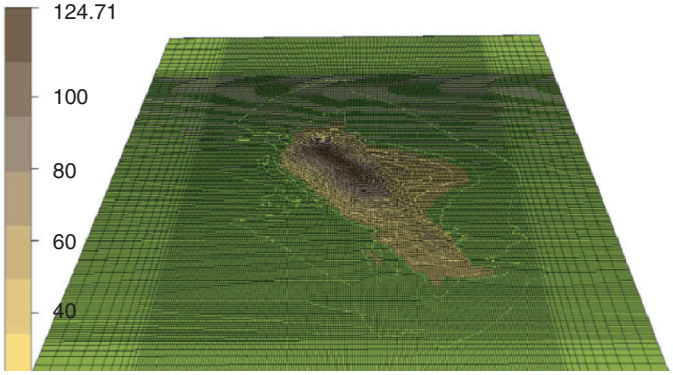

Figure 16: Grid generated for the Askervein Hill along with the elevation map.

Where, $k = 0.41$ is the Von-Karman constant; u^* is the frictional velocity; z_{agl} is the height above the ground level given by $z_{agl} = z - gl\,(gl = 0.75\text{ m})$ and z_0 is the roughness height.

The profiles for turbulent kinetic energy and dissipation rate are taken as follows:

$$k(z) = \frac{u^{*2}}{\sqrt{C_\mu}}\left(1 - \frac{z_{agl}}{h}\right) \tag{22}$$

$$\varepsilon(z) = \frac{u^{*3}}{\kappa}\left(\frac{1}{z_{agl}}\right) \tag{23}$$

Where, h is the boundary layer height. The boundary layer height for the present investigation is set to be 500 m.

3.3.3. Numerical Analysis

The numerical investigations on the Askervein Hill by Castro et al [10] using the standard k-ε model show good agreement with the experimental data. In the present study, a comparison between the three widely used two-equation turbulence models namely the standard k-ε model, the Renormalized Group Theory (RNG) k-ε model and the k-ω model of Wilcox, with experimental data is made. The contours of velocity and turbulent kinetic energy obtained using the present simulation, for the Askervein Hill are presented in Figs. 17 and 18.

A nondimensional speed-up is defined by

$$\Delta S(z) = \frac{V_h(z) - V_{ref}(z)}{V_{ref}(z)} \tag{24}$$

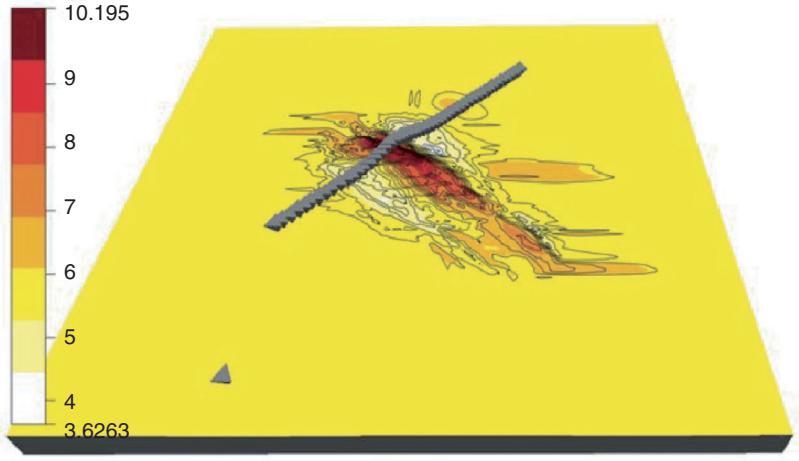

Figure 17: Contours of velocity magnitude ($m^2\,s^{-1}$) at an altitude of 10 m above the surface (ground).

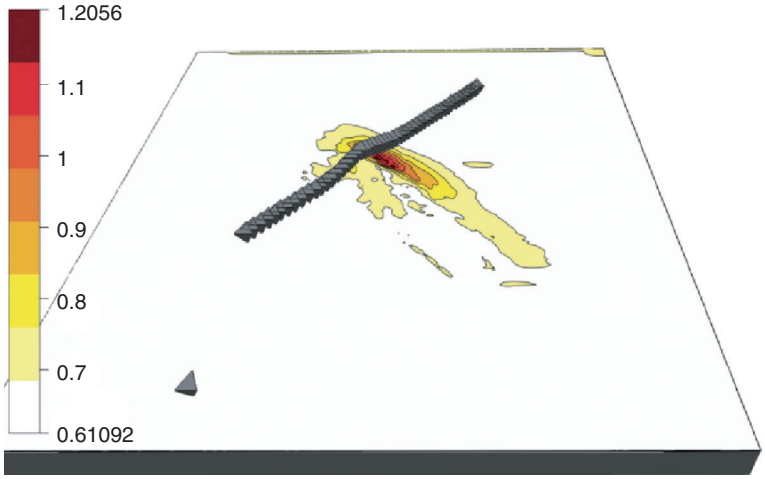

Figure 18: Contours of turbulent kinetic energy ($m^2\,s^{-2}$) at an altitude of 10 m above the surface (ground).

Fig. 19 shows a comparison of the vertical profiles at location "ht" and "Cp" (refer Fig. 11) with available experimental data (from cup and Gill anemometers). The results obtained using the various two-equation models presented in Fig. 19 show that the *k*-omega model predicts velocity magnitudes that are closer to the experimental data. Figure 20 shows a

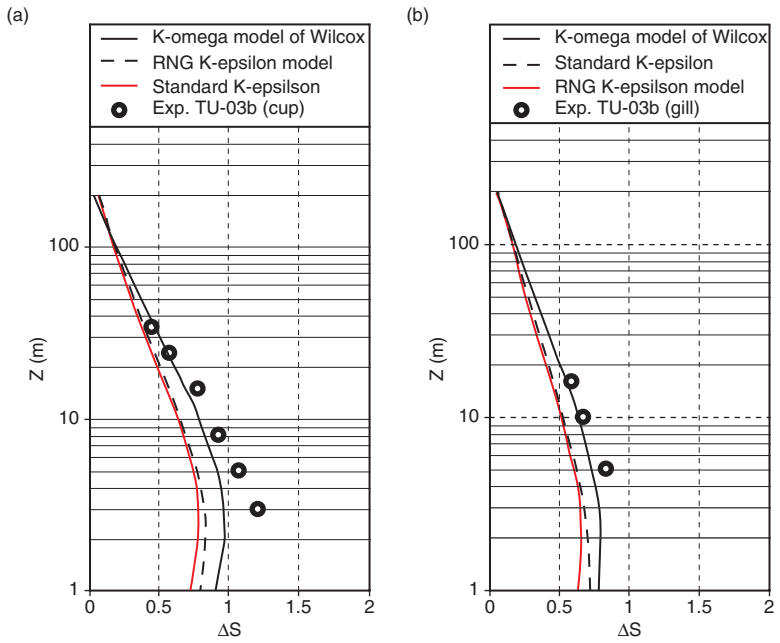

Figure 19: Vertical profile of ΔS at location (a) ht (b) Cp (refer Fig. 9).

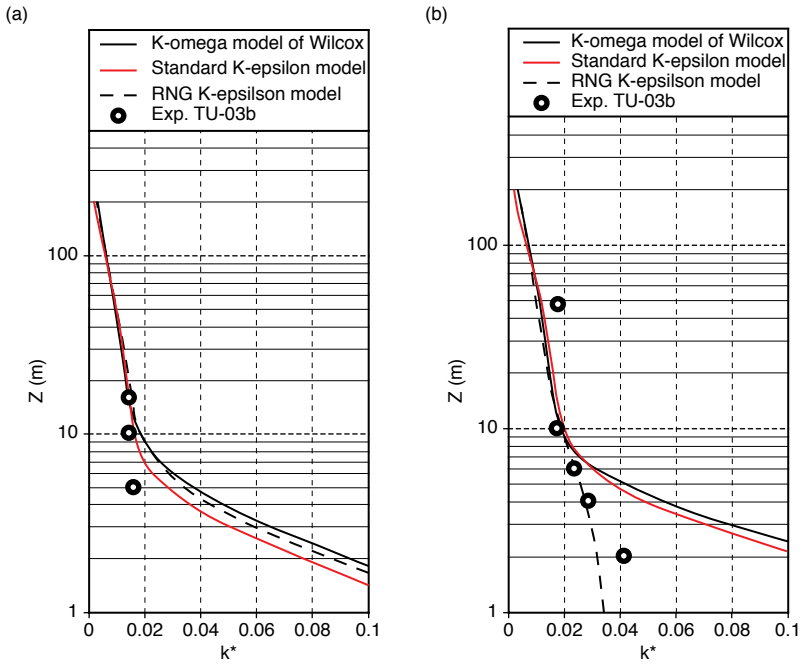

Figure 20: Vertical profile of k* $\left(k^{*}=\frac{k}{v_{ref}^{2}}\right)$ at location (a) ht (b) Cp (refer Fig. 9).

comparison between the non-dimensional kinetic energy $\left(k^* = \frac{k}{v_{ref}^2}\right)$ obtained using the various turbulence models at the locations 'ht' and 'cp'. The vertical profiles obtained using the various models at the location 'ht' are quite similar, whereas the profiles at location 'cp' show that the RNG k-ε model predicts values that are closer to the experimental values. At higher altitudes all the three models considered for the present investigation performs quite well.

CONCLUSIONS

The standard k-ε model, Renormalized Group Theory (RNG) k-ε model and the k-ω model of Wilcox have been validated for flow over complex terrain by comparing the numerical results obtained from the commercial CFD software WindSim V-5.1.0 with the available experimental data. A comparison between the various two-equation models shows that the k-ω model is able to predict the mean velocity and the turbulent kinetic energy those are closer to the measurements. In the case of the Bolund Hill, the Standard k-epsilon & RNG k-epsilon model predicts lower turbulence kinetic energy and thereby under predicts the turbulent intensity. The results obtained using the k-ω model of Wilcox are quite promising but more validation cases are required to confirm that the k-ω model is more suitable for atmospheric boundary layer (ABL) flows. None of the two-equation turbulence models considered for the present investigation could predict the flow behavior on the leeward side of the Hill where the elliptic effects are more pronounced. This might require further investigation using higher order turbulence closure models like the Reynolds Stress Model (RSM), Large Eddy Simulation (LES) or Detached Eddy Simulation (DES) to acquire more in depth information of the flow behavior. From the present study it is clearly evident that computational wind engineering can serve as an effective substitute for expensive experiments if the turbulence models used for flow predictions are properly validated.

REFERENCES

[1] Bitsuamlak T, Stathopoulos T, ASCE F, Bedard, C. Numerical evaluation of wind flow over complex terrain: review. Journal of Aerospace Engineering. 2004; 17 (4): 135–145.

[2] Praveen Kumar P. The effect of Von Karman vortex street on building ventilation. Proceedings of the World Congress on Engineering, Vol II, July 1–3, 2009, London, U.K.

[3] Blocken B, Stathopoulos T, Carmeliet J. CFD Simulation of the atmospheric boundary layer: wall function problems. Atmospheric Environment 2007; 41(2): 238–252.

[4] Arne Reidar Gravdahl. PhD Thesis, Numerical simulations of turbulent flow in complex geometries. PhD Thesis, University of Trondheim, Norwegian Institute of Technology. 1993.

[5] Carpenter P, Locke N. Investigation of wind speed over multiple two dimensional Hills. Journal of Wind Engineering and Industrial Aerodynamics. 1999; 83 (1–3): 109–120.

[6] Bechmann A, Berg J, Courtney MS, R′ehor′e PE, Mann J, Sørensen NN, Risø DTU, National Laboratory for Sustainable Energy, DK-4000 Roskilde, *http://bolund.risoe.dk*

[7] Bechmann A, Berg J, Courtney MS, Jrgensen HE, Mann J, Sorensen NN. The bolund experiment: Overview and background. Technical Report Risø-R1658(EN), Risø DTU, National Lab., Roskilde, Denmark, 2009.

[8] Taylor PA, Teunissen HW. ASKERVEIN'82: Report on the September/October 1982 experiment to study boundary layer flow over Askervein, South Uist, Report: MSRS-83-8,

Technical Report, Meteorological Services Research Branch Atmospheric Environment Service 4905 Dufferin Street, Downsview, Ontario, Canada M3H 5T4.

[9] Taylor PA, Teunissen HW. The Askervien Hill Project: Report on the September/October 1983, main field experiment Report: MSRS-84-6, Technical Report, Meteorological Services Research Branch Atmospheric Environment Service 4905 Dufferin Street, Downsview, Ontario, Canada M3H 5T4.

[10] Castro FA, Palma JMLM, Silva Lopes.A. Simulation of the Askervein flow. Part I: Reynolds averaged Navier-Stokes equations (k-ε turbulence model). Boundary Layer Meteorology 2003; 107: 501–530.